ELECTROMAGNETIC WAVES IN THE IONOSPHERE

The terrestrial ionosphere is a roughly spherical shell of weakly ionized plasma that surrounds the earth. A *plasma* is a gas that has been ionized by radiation or by charged particles, so that it consists of free electrons, ions, and neutrals; it is sometimes referred to as the "fourth state of matter" (1). The main ionizing agents are solar radiation in the extreme ultraviolet (EUV) region, soft X rays, Lyman-α radiation, and hard X rays, as well as cosmic rays. This spherical shell is stratified into distinct layers, the lowest region being the D layer starting at about 50 km height, the E region starting at about 100 km, the F1 layer (during the day) near 250 km, and the F2 layer at about 350 km. At high geomagnetic latitudes, solar energetic charged particles are also important ionizing agents. Figure 1 is a plot of log density versus log kinetic temperature showing the relative state of ionization of various plasmas.

THE RADIO SPECTRUM

A considerable portion of the radio spectrum (ELF through HF) is affected by our ionosphere, as shown in Table 1.

IONOSPHERIC INTERACTION

The basic interaction mechanism between radio (EM) waves and the ionosphere involves the oscillation of the electric component of the wave acting on free electrons, which are $\approx$1800 times less massive than the ionospheric neutrals or ions. The ***E*** wave induces motion of the electrons, and at the same time the ionosphere abstracts energy from the electrons—resulting in a bending of the radio wave and some energy loss from the wave. Figure 2 illustrates the attenuation of radio waves in

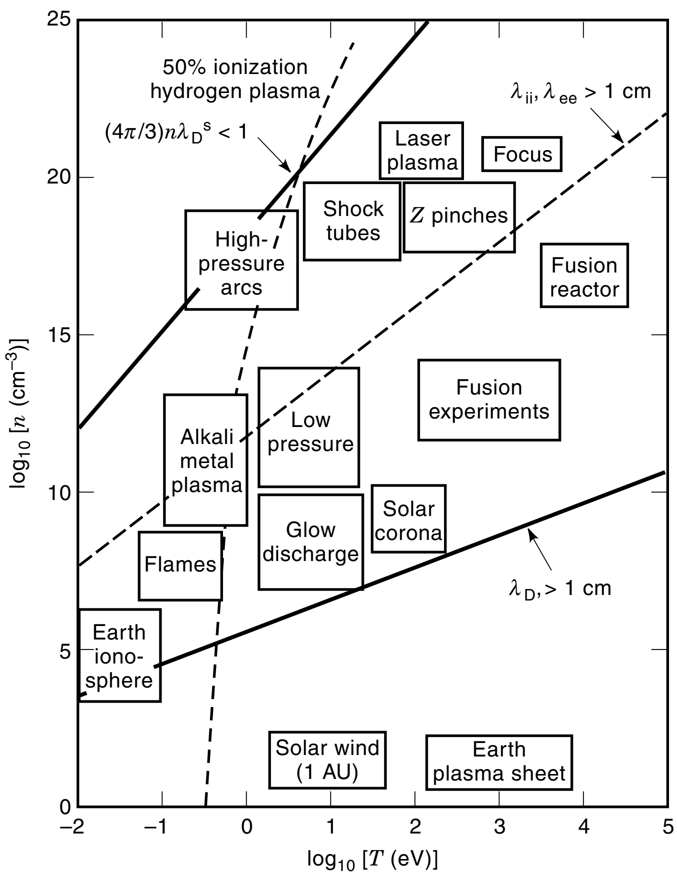

Figure 1. Logarithmic plot of approximate magnitudes of some typical laboratory and natural plasmas.

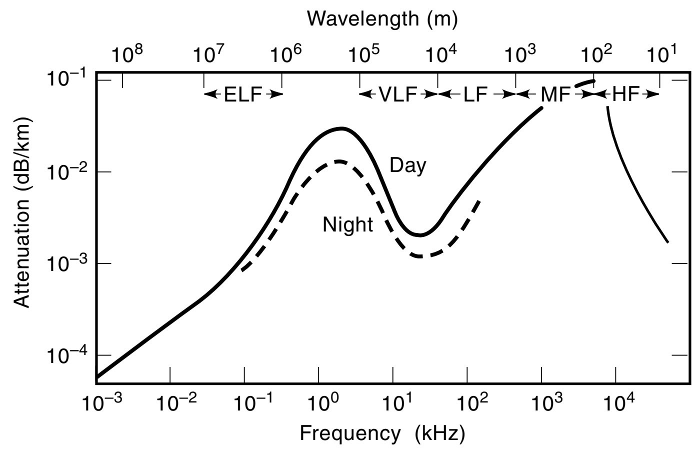

Figure 2. Night–day variation of attenuation on radio paths as a function of frequency from 1 Hz to 30 MHz. (Courtesy of D. Llanwyn Jones.)

the ionosphere as a function of frequency from 1 Hz to 30 MHz.

As may be seen in Fig. 2, there is a variation in radio wave attenuation from day to night. The *virtual height* (the height at which radio waves at vertical incidence are reflected) varies with time of day, with season of the year, and with geomagnetic activity. The most regular variation is the local time variation, as shown in Fig. 3.

There are many techniques used to investigate the characteristics of the ionosphere (2–4). The propagation of radio waves in the ionosphere is described in considerable detail in Ref. 5, and solar–terrestrial relations and their effects on radio propagation are covered in Ref. 6. Radiowave propagation at all frequencies depends to different degrees on the geo-

Table 1. The Radio Spectrum as Defined by the International Telecommunications Union, (ITU); Primary Modes of Propagation, and Effects of the Terrestrial Ionosphere

ITU Designation	Frequency Range	Principal Propagation Modes	Principal Uses
Extra low frequency (ELF)	30–300 Hz	Ground wave and earth–ionosphere waveguide mode	Submarine communication
Very low frequency (VLF)	3–30 kHz	Same as above	Navigation, standard-frequency and -time dissemination
Low frequency (LF)	30–300 kHz	Same as above	Navigation LORAN-C[a]
Medium frequency (MF)	300–3000 kHz	Primarily ground wave, but sky wave[b] at night	AM broadcasting, maritime, aeronautical communication
High frequency (HF)	3–30 MHz	Primarily sky wave, some ground wave	Shortwave broadcasting, amateur, fixed services
Very high frequency (VHF)	30–300 MHz	Primarily LOS,[c] some sky wave at lower VHF	FM broadcasting, television, aeronautical communication
Ultra high frequency (UHF)	300–3000 MHz	Primarily LOS, some refraction and scattering by the ionosphere	Television, radar, navigation,[d] aeronautical communication
Super high frequency (SHF)	3–30 GHz	Same as above	Radar, space communication

[a] The LORAN-C system will probably be superseded by the GPS system.
[b] Sky wave denotes the earth–ionosphere–earth reflection mode.
[c] Line of sight.
[d] Global Positioning System satellite constellation.

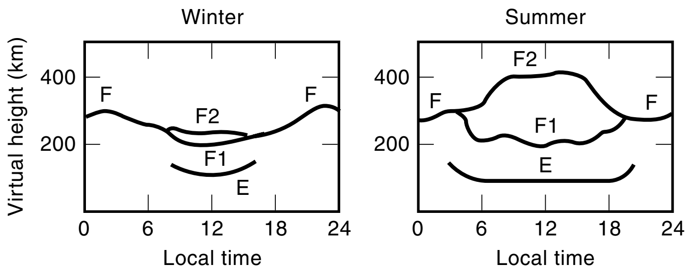

Figure 3. Average variation of ionospheric layer height as a function of season and local time. Note the large change in height of the F2 layer in summer.

graphic and geomagnetic latitudinal region of the ionosphere. The most benign latitudinal region is the *midlatitudes;* the most disturbed regions are the *auroral, equatorial,* and *polar* regions, as described in detail in Ref. 7. In the next section we describe qualitatively the salient propagation modes and ionospheric effects on radio waves as a function of frequency. The section after provides a mathematical description and the physical principles of the interaction of radio waves with the ionosphere. The final section will introduce the reader to the frontiers of ionospheric research at the end of the twentieth century.

EFFECTS UPON SPECIFIC RADIO SERVICES

Extremely Low and Very Low Frequencies

As indicated in Table 1, at the lowest frequencies (ELF–VLF) the basic propagation mode is a spherical *waveguide mode,* with the D and E regions of the ionosphere forming the upper boundary, and the surface of the earth the lower boundary. A simplified earth–ionosphere waveguide geometry is shown in Fig. 4 (8). A schematic diagram of the first two waveguide modes in an ideal earth–ionosphere mode is presented in Fig. 5.

In reality, the ELF–VLF waveguide mode is considerably more complicated because of its spherical nature and the electrical characteristics of the upper and lower boundaries. At ELF frequencies, the wavelength is of the same order of magnitude as the transverse dimensions of the waveguide, and the signal propagates deeply into both land and sea because of the "skin depth" effect.

At global distances, the signal is very stable, but extremely long antennas and high transmitter powers are required and the signaling rate is extremely slow. One unique advantage of ELF is the ability of the signal to penetrate relatively deeply into sea water (at 100 Hz, the attenuation in sea water is 0.3 dB/m, which is $\approx\frac{1}{3}$ of the attenuation in the waveguide). The attenuation of ELF signals penetrating normal earth is approximately $\frac{1}{10}$ of that in sea water, so ELF signals can be used to probe or communicate into the solid earth. There is also some evidence that high latitude effects such as D-region irregularities can cause some phase anomalies in ELF and VLF transmissions (9).

VLF (3 kHz to 30 kHz) transmissions also require large antennas and high-power transmitters, but are used more than ELF for time- and frequency-standard dissemination and navigational systems. VLF signals are also influenced by anomalies on the earth's surface (10) and in the high-latitude ionosphere (4,5).

Low Frequencies

Moving up in frequency to the LF band (30 kHz to 300 kHz), the basic propagation mode below $\approx$100 kHz is by the ground (surface) wave, which follows the earth's curvature, and above 100 kHz is the sky wave and the waveguide mode. The sky wave is, of course, influenced by the ionospheric diurnal, seasonal, and latitudinal variations.

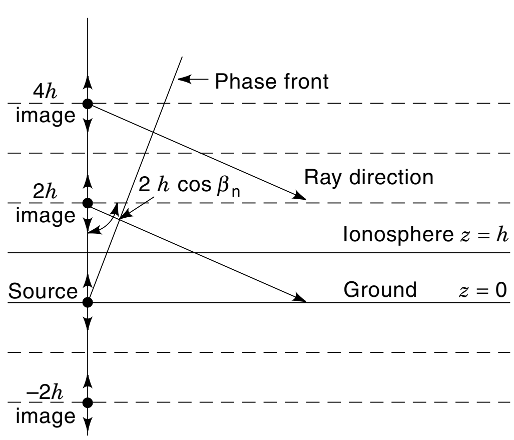

Figure 4. Simplified ray geometry for the first-order and second-order VLF–ELF modes. The two conducting planes are representative at the earth surface and the ionosphere.

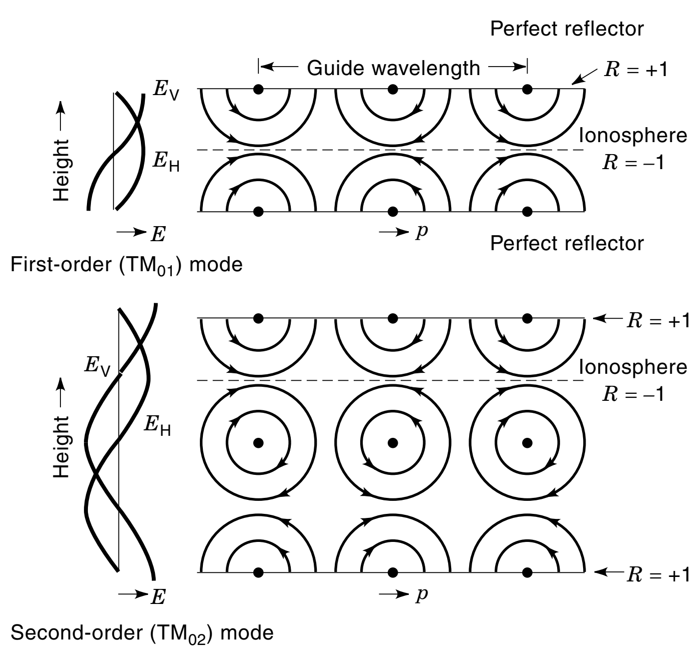

Figure 5. The ***E*** field for ideal earth–ionosphere waveguide modes.

Medium Frequencies

Propagation during the daytime in the MF (300 kHz to 3000 kHz) band is by ground wave, and for frequencies at night above ≈500 kHz by sky wave. At geomagnetic latitudes greater than ≈55°, the auroral ionosphere introduces some anomalous sky-wave propagation modes (11).

High Frequencies

The ionosphere has the most profound effect on signals in the HF (3 MHz to 30 MHz) band, making the sky-wave mode the dominant means of propagation. The ground wave at HF is sometimes used in the frequency range of 3 MHz to 6 MHz, especially over sea water, whose conductivity is much greater than that of ordinary land. At HF wavelengths relatively high efficiency, gain, and directivity can be achieved in the antenna systems, so directive communications and broadcasting are realizable. Above 6 MHz, the sky wave is dominant, so one must really understand ionospheric behavior and phenomenology in order to predict propagation. Since the ionosphere varies with time of day, season, solar activity, and sunspot cycle, predicting HF propagation over a specific path can be somewhat complicated. Propagation paths up to ≈10,000 km are quite common for shortwave (SW) broadcasters, who use antennas with gains of up to 20 dBi (dBi is referenced to an isotropic source) and transmitter powers of 250 kW and higher. With much less reliability, amateur radio operators ("hams") sometimes also achieve two-way communications over similar path lengths using antenna gains of ≈3 dB to 12 dB and transmitter powers of 5 to 1000 W.

The ionosphere also behaves differently in the equatorial, midlatitude, auroral, and polar latitudinal regions. Fortunately, several fairly reliable and easy-to-use HF propagation prediction programs are now available for PCs (IONCAP, ASAPS, VOACAP, AMBCOM, etc.). The sources of these programs may be found in recent books and articles (5,12–14) and in the amateur radio magazines (*QST, CQ, World Radio*). Unfortunately, none of the existing prediction programs gives very reliable results in the auroral regions. A following section describes the essentials of ionospheric propagation in considerable detail.

Very High Frequencies

Propagation in the VHF band (30 MHz to 300 MHz) is primarily by line of sight (LOS) to the optical horizon, so if the antenna patterns direct most of the RF power in the horizontal plane, there are essentially no ionospheric effects. For earth–space propagation paths, however, the ionosphere can affect the signal adversely by refraction, diffraction, scattering, or reflection. These effects can be especially important when the path traverses the equatorial, auroral, and polar ionosphere. The amplitude, phase, and polarization of the signal may change measurably. These effects will be quantified in the following section.

Extrahigh Frequencies

At EHF and above, propagation is primarily LOS, and because of the higher frequencies ($f \gtrsim 300$ MHz), these signals are less affected by the ionosphere than lower frequencies. On earth–space paths that traverse the equatorial and/or high-latitude ionosphere, however, the signal quality can be significantly degraded. These effects will be described below.

To summarize, the radio services *most* affected by the ionosphere lie in the frequency range of ≈1 MHz to 150 MHz [fixed communication services, AM (amplitude modulation) and SW (shortwave) broadcasting, amateur radio]. To a lesser degree, services in the 20 kHz to 300 MHz region (mainly some of the navigation services] suffer some ionospheric perturbation effects.

There is a plethora of radio instrumentation currently deployed globally that operates routinely or on a campaign basis to measure characteristics of the terrestrial ionosphere. It is beyond the scope of this article to describe these techniques, but they have been described in considerable detail in the literature (2–4).

PHYSICAL PRINCIPLES AND MATHEMATICAL DESCRIPTION OF ELECTROMAGNETIC INTERACTION WITH THE IONOSPHERE

Because of the complexity of the terrestrial ionosphere (a weakly ionized plasma with a superimposed magnetic field in which electric currents flow), we must utilize the magnetoionic theory to quantify the ionosphere physical parameters. The most successful formulation of the appropriate magnetoionic theory was derived by Appleton and others in the mid-1920s (15–17). We can obtain some first-order properties of the ionosphere by ignoring the magnetic field (18). A simple dispersion equation for electromagnetic (EM) waves in the ionosphere is

$$\mu = \sqrt{1 - \frac{Ne^2}{\pi m f^2}} \tag{1}$$

where

μ = refractive index of the ionosphere (real part of the complex refractive index n)
N = electron number density of the ionosphere (e/cm^3 or e/m^3)
e = electronic charge = 1.6×10^{-19} C
m = mass of the electron = 9.1×10^{-31} kg
f = frequency of the radio wave in the ionosphere (Hz)

For reflection at vertical incidence, $\mu = 1$ and

$$\begin{aligned} N &= m\pi f^2/e^2 \\ &= 1.24 \times 10^4 f^2 \text{ e/cm}^3 \qquad (f \text{ in MHz}) \\ &= 1.24 \times 10^{10} f^2 \text{ e/m}^3 \qquad (f \text{ in MHz}) \end{aligned} \tag{2}$$

Another useful quantity is the plasma frequency,

$$\begin{aligned} f_n &= \sqrt{\frac{Ne^2}{\pi m}} \\ &= 9\sqrt{N}\,\text{kHz} \qquad (N \text{ in cm}^{-3}) \\ &= 9 \times 10^{-3}\sqrt{N}\,\text{MHz} \qquad (N \text{ in } e/\text{cm}^3) \end{aligned} \tag{3}$$

The Virtual Height Concept

If we consider an RF pulse traveling vertically upward into the ionosphere at the speed of light, $v = c$, it will be reflected at the *virtual height, h'*. The time required for the pulse to be reflected from an ionospheric layer and return to the earth is

$$t = \frac{2}{c}\int_0^h \frac{dz}{\mu} \quad (4)$$

then the virtual height can be found from $h'(f) = \frac{1}{2}$ ct, or

$$h'(f) = \int_0^h \frac{dz}{\sqrt{1 - f_n^2/f^2}} \quad (5)$$

Since the pulse always travels more slowly in the layer than in free space, the virtual height of a layer is always greater than the true height. The true height and virtual height are related by the integral equation

$$h'(f) = \int_0^{Z_{\max}} \frac{dz}{\mu(f, z)} \quad (6)$$

where z is the *true height,* $Z_{\max}$ is the maximum height reached by the frequency f, and n is the refractive index at $Z_{\max}$ for the frequency f. A good discussion of the relation between true height and virtual height is given in Ref. 19.

Vertical and Oblique Propagation

Before considering the behavior of a radio signal in a magnetoionic medium, we will state three theorems that relate oblique and vertical incidence propagation as depicted in Fig. 6. The first is the *secant law,* which relates the vertical-incidence frequency f_v reflected at B to the oblique-incidence frequency f_{ob} reflected at the same true height. A typical derivation of this relation is given in Ref. 5, and it is usually written as

$$f_{ob} = f_v \sec \phi_0 \quad (7)$$

The secant law, then, relates the two frequencies f_v and f_{ob} reflected from the same true height (the distance BD in Fig. 6).

In order to determine sec ϕ and f_{ob} values from vertical-incidence soundings (which measure the virtual height h'), we need two more theorems. *Breit and Tuve's theorem* states that the time taken to traverse the actual curved path *TABCR* in Fig. 6 at the group velocity v_g equals the time necessary to travel over the straight-line path *TER* at the free-space velocity c. Referring to the geometry shown in Fig. 6, we can write the expression

$$\begin{aligned} t &= \frac{1}{c}\int_{TER} \frac{dx}{\sin \phi_0} \\ &= \frac{D}{c} \sin \phi_0 \\ &= \frac{TE + ER}{c} \end{aligned} \quad (8)$$

Martyn's theorem may be written concisely as

$$h'_{ob} = h'_v \quad (9)$$

Smith (20) devised a set of logarithmic transmission curves, parametric in range, for the curved earth and ionosphere. They are shown in Fig. 7 and are sufficiently accurate for the distances shown.

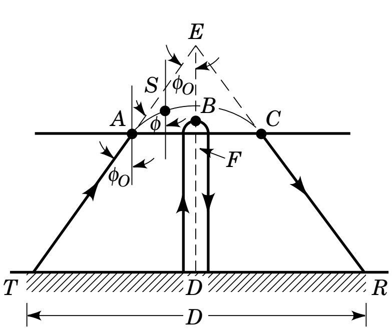

Figure 6. Plane geometry describing vertical and oblique ionospheric propagation.

Radio Propagation in a Magnetized Plasma

Before proceeding with a discussion of the Appleton (magnetoionic) equations, we need to define two quantities contained explicitly in the equations. The first is ν, the number of collisions per second (collision frequency) between electrons and heavier particles (ions and neutrals). Another quantity, the *gyromagnetic frequency* or *gyrofrequency,* is the natural frequency (Hz) of gyration of an ion or electron in a magnetic field of strength B_0 (Wb/m^2) and is given by

$$f_H = \frac{|e|}{2\pi m} B_0 \approx 2.80 \times 10^{10} B_0 \quad (10)$$

and the *angular* gyrofrequency is given by

$$\omega_H = \frac{|e|}{m} B_0 \approx 1.76 \times 10^{11} B_0 \quad (11)$$

Since electrons are much less massive than ions, the electron gyrofrequency affects the propagation of HF waves in the ionosphere more than the ion gyrofrequencies. For example, since $B \approx 0.5 \times 10^{-4}$ Wb/m^2, the electron gyrofrequency is $\approx$1.40 MHz, which falls at the upper end of the medium wave band.

The Dispersion Relation. Using the recommended URSI (International Union at Radio Science) notation, the magnetoionic dispersion equation for a radio wave in a homogeneous, partially absorbing ionized gas upon which a constant magnetic field is impressed is given by

$$n^2 = 1 - \cfrac{X}{(1 - jZ) - \left[\cfrac{Y_T^2}{2(1 - X - jZ)}\right] \pm \left[\cfrac{Y_T^4}{4(1 - X - jZ)^2} + Y_L^2\right]^{1/2}} \quad (12)$$

where

n = *complex* refractive index = $(\mu - j\chi)$
ω = angular frequency of the exploring wave (rad/s)

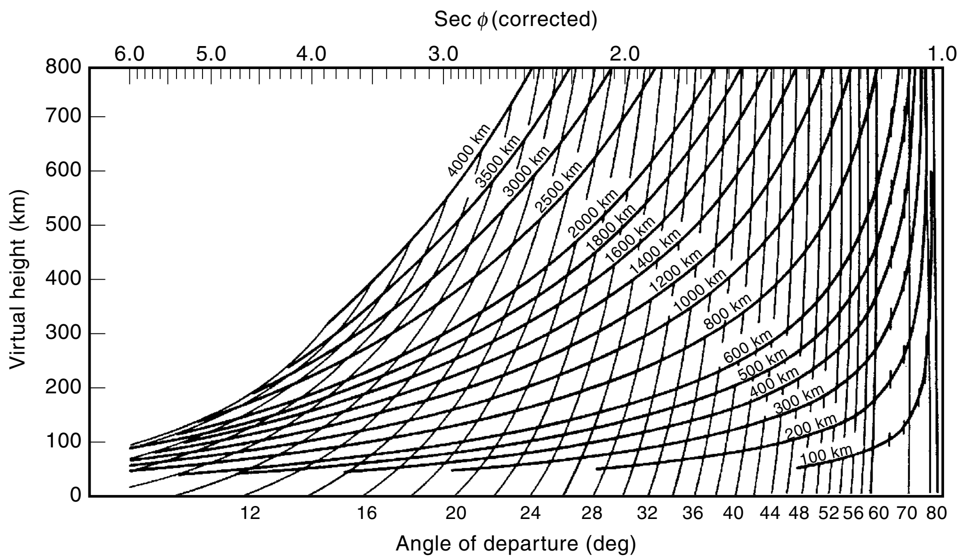

Figure 7. Logarithmic transmission curves for curved earth and ionosphere, parametric in distance between transmitter and receiver.

ω_N = angular plasma frequency
ω_H = angular gyrofrequency = $B_0|e|/m$ (rad/s)
ω_L = longitudinal angular gyrofrequency = $(B_0|e|/m)\cos\theta$
ω_T = transverse angular gyrofrequency = $(B_0|e|/m)\sin\theta$
$X = \omega_N^2/\omega^2$
$Y = \omega_H/\omega$
$Y_L = \omega_L/\omega$
$Y_T = \omega_T/\omega$
$Z = \nu/\omega$
θ = angle between the wave-normal and the magnetic field inclination

The Polarization Relation. We begin by defining the *polarization ratio* R as

$$R = -H_y/H_x = E_x/E_y \tag{13}$$

Then we can write the double-valued polarization equation as

$$R = -\frac{j}{Y_L}\left[\frac{1}{2}\frac{Y_T^2}{1-X-jZ} \mp \left(\frac{1}{4}\frac{Y_T^4}{(1-X-jZ)^2} + Y_L^2\right)^{1/2}\right] \tag{14}$$

In the upper F region of the ionosphere where the electron–ion collision frequency is very low, we may simplify the dispersion and polarization equations by dropping the Z term (since $\nu \approx 0$). Equations (12) and (14) then become (for no absorption)

$$n^2 = 1 - \frac{2X(1-X)}{2(1-X) - Y_T^2 \pm [Y_T^4 + 4Y_L^2(1-X)^2]^{1/2}} \tag{15}$$

and

$$R = -\frac{H_y}{H_x} = -\frac{j}{Y_L}\left(1 + \frac{X}{n^2-1}\right) \tag{16}$$

If we further simplify Eq. (12) by dropping the Y terms (no magnetic field), then we obtain $n^2 = 1 - X$, which is equivalent to Eq. (1).

According to magnetoionic theory, a plane-polarized EM wave traveling in a medium like the terrestrial ionosphere will be split into two *characteristic waves.* The wave that most closely approximates the behavior of a signal propagating in this medium, *without* an imposed magnetic field, is called the *ordinary* wave, and the other is called the *extraordinary* wave. These terms are taken from the nomenclature for double refraction in optics, although the magnetoionic phenomena are more complicated than the optical ones. The ordinary wave is represented by the upper sign in the polarization Eq. (14), except when the wave-normal is exactly along the direction of the magnetic field. Anomalous absorption occurs for the extraordinary wave when its frequency equals the electron gyrofrequency ($f_H = |B|\ e/m_e \approx 0.8$ to 1.6 MHz). These frequencies lie in the medium-frequency (MF) band; consequently the absorption of the extraordinary wave [$A \approx (f - f_H)^2$] is large and the polarization of the transmitted wave is important in the determination of the fraction of the incident power that goes into the extraordinary wave. This is especially true near the dip equator, where the magnetic field is nearly horizontal and the field is usually vertical.

In addition to anomalous absorption effects near the electron gyrofrequency, the wave may also experience significant lateral deviation. This is illustrated for vertical and oblique propagation in Sections 11.2.2 through 11.2.4 of Ref. 5.

If Eq. (16) is recast as a funtion of ω and we define $f(\theta) = \frac{1}{2}(\sin^2\theta)/\cos\theta$ and $\omega_c = (B_0|e|/m)\,f(\theta)$, then it will be seen to describe an ellipse. The quantities $f(\theta)$ and ω_c play an important part in the description of the polarization behavior of waves in magnetoionic theory. The *magnitude* of ω_c is independent of frequency, but varies with the angle between the wave normal and the magnetic field, θ, whereas the *sign* of ω_c depends on the sign of the charge e and on the direction of the magnetic field. For longitudinal propagation $\omega_c = 0$, and for transverse propagation $\omega_c \to \infty$. In the case where $X = 1$, the quantity ω_c primarily determines the polarization of the wave. A very complete discussion of R as a function of X and of the variation of the polarization ellipse is given in Ref. 21.

A more complete understanding of the behavior of EM waves in the terrestrial ionosphere may be obtained by employing two approximations. The *quasilongitudinal* (QL) approximation applies when the wave is propagating nearly parallel to the geomagnetic field, and the *quasitransverse* (QT) approximation applies when the wave propagates in a direction nearly normal to the geomagnetic field. References 21 and 22 contain extended discussions of the QL and QT approximations:

$$\text{QT: } Y_T^4 \gg 4(1-X)^2 Y_L^2$$
$$\text{QL: } Y_T^4 \ll 4(1-X)^2 Y_L^2$$

Absorption of Radio Waves in the Ionosphere

The refractive index n is modified when one introduces collisions between the electrons and heavy particles, and the wave experiences *absorption,* which physically is due to the conversion of ordered momentum into random motion of the particles after collision. For each collision, some energy is transferred from the EM wave to the neutral molecules and appears as thermal energy. We will follow the standard treatment of absorption of radio waves in the ionosphere presented by Davies (22) and Budden (23).

For the propagation of an EM wave in an *unmagnetized* plasma, we can define the absorption index (or coefficient) as

$$K = \frac{\omega}{c}\chi \tag{17}$$

where χ is the imaginary part of the refractive index n. For a magnetized plasma without collisions, we can write

$$K = \frac{e^2}{2\epsilon_0 mc\mu}\cdot\frac{N\nu}{\omega^2+\nu^2} \tag{18}$$

On this basis, we can conveniently divide absorption into two limiting types, commonly called *nondeviative* and *deviative* absorption. Nondeviative absorption occurs in regions where the product $N\nu$ is large and $\mu \approx 1$, and is characterized by the absorption of HF waves in the D region. Deviation absorption, on the other hand, occurs near the top of the ray trajectory or anywhere else on the ray path where significant bending takes place (for small $N\nu$ and $\mu < 1$).

When the refractive index ≈1, there is essentially no bending of the ray and we can write

$$K \approx 4.6\times10^{-2}\frac{N\nu}{\mu(\omega^2+\nu^2)}\ \text{dB/km} \tag{19}$$

We can further simplify Eq. (19) for the VHF case, since $\omega^2 \gg \nu^2$, as

$$K = 1.15\times10^{-3}\frac{N\nu}{f^2}\ \text{dB/km} \tag{20}$$

In the MF and HF bands, Eq. (19) may be written as

$$K = 4.6\times10^{-2}\frac{N}{\nu}\ \text{dB/km} \tag{21}$$

Unlike nondeviative absorption, deviative absorption occurs when the wave experiences significant group retardation and consequently spends a relatively long time in the absorbing layer and there is considerable curvature of the ray path. The general expression for the absorption index in a deviating region of a nonmagnetic plasma is

$$K = \frac{\nu}{2c\mu}(1-\mu^2-X^2) \tag{22}$$

In the ionosphere, Eq. (22) reduces to

$$K = \frac{\nu}{2c}\mu' \tag{23}$$

where μ' is the group refractive index. For large values of μ', we can write the preceding equation as

$$K = \frac{\nu}{2c}\frac{X}{\sqrt{1-X}} \tag{24}$$

We should remember that the concepts of deviative and nondeviative absorption are limiting cases, and that as a wave approaches the reflecting level, ray theory breaks down, so we must employ full wave theory to obtain a complete description of the behavior of the wave. Extended discussions of application of the QL and QT approximations to ionospheric absorption may be found in Refs. 2, 5, and 23.

Scattering of Radio Waves in the Ionosphere

The principles of scattering of radio waves in general are discussed in the articles ELECTROMAGNETIC WAVE SCATTERING AND BACKSCATTER. One can qualitatively describe ionospheric scattering as either *strong* or *weak* in terms of the received signal strength of the scattered signal at the receiving radar antenna. An example of the former is VHF–UHF backscatter echoes received from electron density gradients in the auroral E region, and an example of the latter is incoherent backscatter received by a VHF–UHF radar from the undisturbed E or F layer.

Another way of classifying scattered echoes is in terms of their *backscatter cross section* σ (using a pulsed radar system) and their *temporal stability.* A *coherent* echo exhibits a statistical correlation of the amplitude and phase from one pulse to another and emanates from quasideterministic gradients in electron density, which have correlation times usually greater than 1 ms, corresponding to a spectral width of the radar echo of less than 1000 Hz (sometimes less than 100 Hz). It also has a backscatter cross section 10^4 to 10^9 times than that from an incoherent echo. Other important considerations in the case of coherent backscatter are the relation between the scattering-irregularity size relative to the backscatter sounder free-space wavelength, the mean fractional deviation in electron density of the scatterer, and the aspect angle between the radar line of sight and the major axis of the irregularity. On the other hand, an *incoherent* echo arises from random thermal fluctuations in the ionosphere, which have typical correlation times of ≈20 μs, corresponding to a radar echo spectral width of ≈50 kHz.

The physical principles governing coherent and incoherent scattering from the ionosphere are covered in Refs. 2, 5, and 6, while plasma wave theory is covered in detail in Ref. 8, and extended descriptions of techniques for studying the ionosphere using coherent- and incoherent-scattering sounders are given in Refs. 2, 3, 5, and 6.

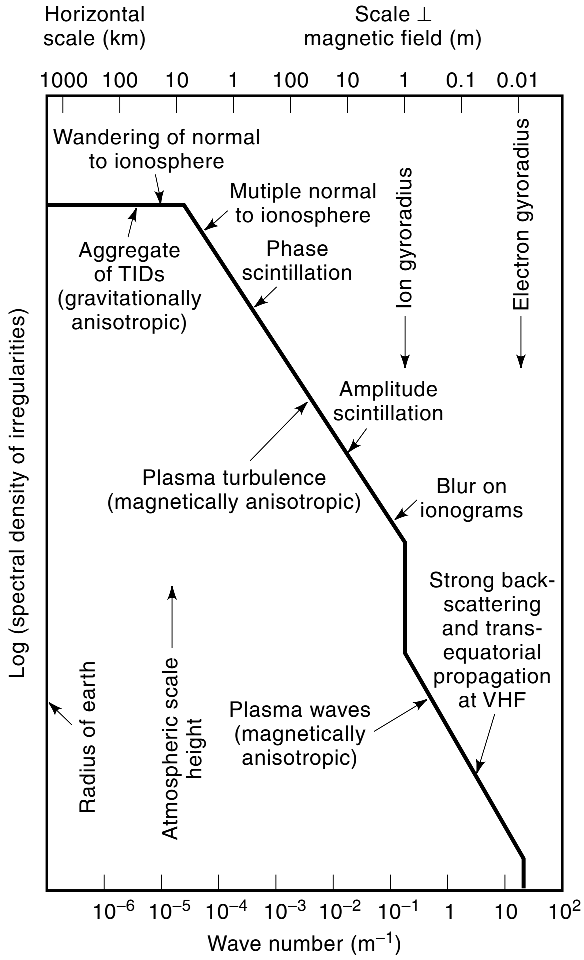

Figure 8. Composite spectrum of ionospheric irregularities as a function of wave number over a large spatial scale. (Courtesy of H. G. Booker.)

Because of charged particle precipitation of solar origin, ionospheric electric currents and fields, and plasma dynamics, there exists a wide spectrum of scale sizes of ionospheric irregularities, as shown in Fig. 8. Irregularities are most prevalent at auroral, polar, and equatorial latitudes, although they also exist at midlatitudes (24). The global morphology of ionospheric irregularities is covered in Refs. 4–7.

Ionospheric Scintillation

Ionospheric scintillations are fluctuations of amplitude, phase, and angle of arrival of a VHF–UHF signal passing through irregularities located mainly in the F region. Ionospheric scintillations can have deleterious effects on satellite-based communication and navigation systems. Either extragalactic sources (such as radio stars) or satellite beacon transmitters may be used as the signal sources for earth-observed studies of ionospheric scintillations, and both geostationary and orbiting satellite beacons have been used. There is a voluminous body of literature since 1970 describing the theory, technique, and results of ionospheric scintillation measurements (2–5).

Faraday Rotation

One physical principle that makes possible the determination of ionospheric columnar electron content is Faraday rotation. This effect (for optics) was discovered by Michael Faraday in 1845, when he subjected a block of glass to a strong magnetic field. He observed that a plane-polarized monochromatic beam of light passing through the glass in a direction parallel to the imposed magnetic field has its plane of polarization rotated. The amount of rotation is given by the expression

$$\Omega = KHl \tag{25}$$

where

Ω = angle of rotation
K = constant associated with each substance
l = length of path of light through the substance (m)
H = magnetic field intensity (A/m)

The Faraday rotation of the electric vector of a radio wave (see Ref. 45) propagating from a satellite radio beacon in a direction parallel to the earth's magnetic field (as seen by an observer looking up, in the northern hemisphere) is counterclockwise, as shown in Fig. 9.

Ignoring refraction, the Faraday rotation of the electric vector is given by

$$\Omega = \frac{\pi f}{2c} \int_R^S X \sqrt{\frac{Y_T^4 + 4(1-X)^2 Y_L^2}{(1-X)(1-Y_L^2) - Y_T^2}}\, ds \tag{26}$$

where

Ω = Faraday rotation (rad/s)
f = wave frequency (Hz)
c = 2.998 × 10⁸ m/s
$X = kN/f^2$
k = 80.61
N = electron density (e/m³)

and Y_L, Y_T are as previously defined.

The integration is between the receiver R, and the satellite S. For VHF frequencies the QL approximation holds and we can express Eq. (26) as

$$\Omega = \frac{\pi K}{cf^2} \int_R^S f_L N\, ds \tag{27}$$

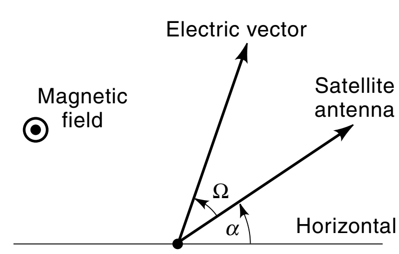

Figure 9. Simplified plane geometry of satellite–earth propagation path in the northern hemisphere to explain Faraday rotation effects.

where $N\,ds$ is the ionospheric electron content. Evaluating the constants yields the relation

$$\Omega \approx 8.447 \times 10^{-7} f^{-2} \int_R^S f_L N\, ds \,\text{rad} \tag{28}$$

where $f_L = 2.80 \times 10^{10} B_L$, the electron gyrofrequency corresponding to the longitudinal component of the geomagnetic field along the ray path.

Details of the application of Faraday rotation theory and other techniques to deduce ionospheric columnar electron content may be found in Refs. 2, 5, and 6.

Whistlers

Whistlers are bursts of EM radiation at VLF that are initiated by lightning discharges and then travel though the ionosphere and magnetosphere in ducts approximately parallel to geomagnetic lines of force. When translated into sound waves, whistlers are distinguished by tones of decreasing (or sometimes increasing) frequency, and they may easily be detected by connecting a suitable antenna to the input of a very sensitive audio amplifier. As a matter of fact, whistlers were first observed in the last years of the nineteenth century, and were also heard on the primitive field telephone systems used in World War I. They have been studied intermittently since 1898, basically as a diagnostic probe of the ionosphere and magnetosphere (2,25). A graphical representation of whistler behavior is shown in Fig. 10, and the somewhat rarer *nose whistler* behavior is illustrated in Fig. 11. The dispersion relation for whistlers is

$$T = \frac{1}{2c} \int_s \frac{f_N f_L\, ds}{f^{1/2}(f_L - f)^{3/2}} = \frac{D}{f^{1/2}} \tag{29}$$

where

D = dispersion = $(1/2c) \int_s (f_N/f_L^{1/2})$ ds
f_N = plasma frequency
f_L = longitudinal component of the plasma frequency

This is the time T for a signal burst to go from one hemisphere to its conjugate point in the opposite hemisphere.

Other natural VLF emissions (called *dawn chorus, risers, hiss,* etc.) that are thought to originate in the ionosphere can also be heard on whistler detection equipment. Since the 1960s, high-power VLF transmitters have been used to *generate* whistlers to study properties of the magnetosphere (26–28).

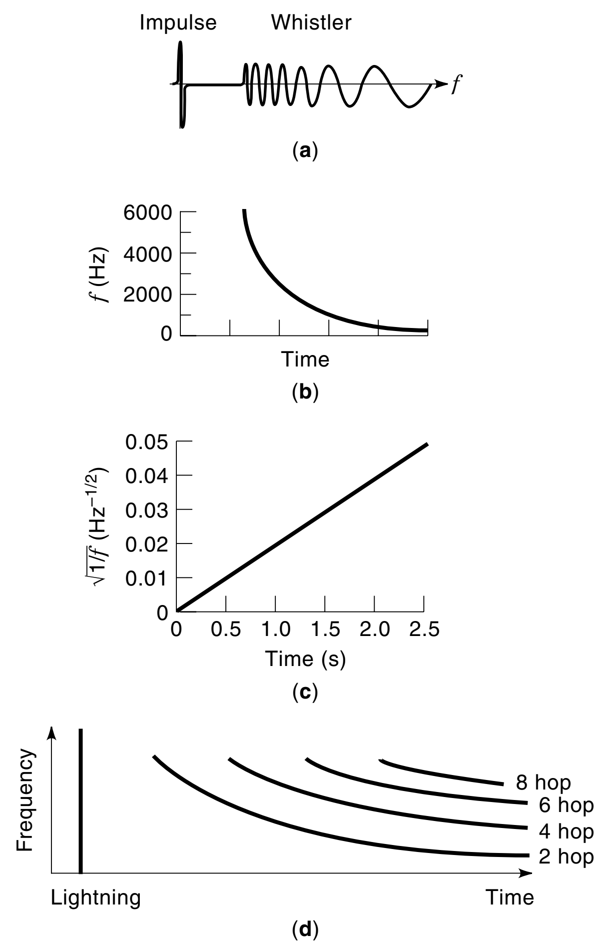

Figure 10. Sketch of basic manifestations of a whistler and its initiating disturbance. (a) The frequency spectrum. (b) Frequency–time curve of a typical whistler. (c) Curve of $\sqrt{1/f}$ with time. Initiating disturbance and multiple hops when the source and receiver are at the same end of a magnetic line of force. [After Helliwell (25).]

FRONTIERS OF IONOSPHERIC RESEARCH

The use of radio waves to explore the terrestrial ionosphere began with the pioneering efforts of Appleton and of Breit and Tuve in 1926, when they independently used different techniques to detect the ionospheric layers. Their work was founded on Marconi's demonstration of transatlantic radio transmission and on the hypotheses of Kennelly and Heaviside, who independently in 1922 postulated that there must be radio-reflecting layers in the upper atmosphere to explain certain experimental results. The foregoing discoveries rested upon the bedrock of the experimental and theoretical work of Heinrich Hertz (1893) and James Clerk Maxwell (1873) respectively.

There seems to have been several peaks in the history of ionospheric research: first, in the 1920s, following World War I; second, starting shortly after the end of World War II; and third, perhaps, starting in the mid-1970s with the advent of digital techniques, and more recently with the advent of the National Space Weather Program (see Ref. 29 or 30 or http://www.nsf.gov/spaceweather/).

While much of the ionospheric research up until about 1960 was in support of HF communications, the advent of satellite communications changed the emphasis to ionospheric

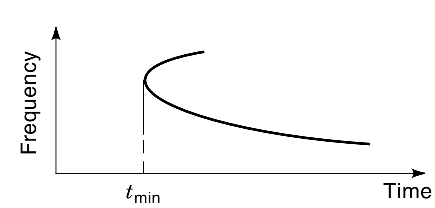

Figure 11. Idealized sketch of the frequency-versus-time characteristics of a nose whistler. [After Davies (5).]

research concerning the effects of the ionosphere on transionospheric propagation and research relating the ionosphere to the magnetosphere. Most current ionospheric research is related to the interrelationship and coupling between regions over the entire height region of the terrestrial atmosphere from the troposphere to the magnetosphere and through interplanetary space to the sun.

There are several areas of ionospheric research that currently seem to be producing exciting new results, and these areas will probably continue to be emphasized well into the twenty-first century. These areas include (not necessarily in order of importance) ionospheric modification by using high-power HF transmissions, ionospheric imaging, coherent radars operating from HF through VHF, and incoherent scattering radars (2–5). Most of these techniques are employed at high geomagnetic latitudes as part of the Space Weather Program, but some are also deployed in equatorial regions. We will briefly describe the essentials of each of these areas of current ionospheric research emphasis.

Ionospheric Modification

In the late 1960s the availability of military surplus equipment such as very high-voltage and -current power supplies and HF vacuum tubes capable of many kilowatts of RF output, together with advances in antenna array theory and practice, induced experimenters to design systems to *heat* or otherwise modify the ionosphere. As a result of experiments performed in the early 1970s at the Platteville, Colorado HF high-power heating facility (31), some 10 new ionospheric modification facilities were established and have produced significant results (see Chap. 14 of Ref. 5). The various modification facilities are listed in Table 2. Other ionospheric modification facilities are located in Russia and Ukraine at Kharkov, Moscow, Zimenki, and Monchegorsk. More information on the HAARP and other heaters may be obtained on internet at http://www.haarp.alaska.edu/haarp/airf.html.

Ionospheric Imaging by Radio

For over three decades now, ionospheric scientists have investigated using radio methods to image the ionosphere. Rogers (32) was probably the first to suggest using the wavefront-reconstruction method for this purpose. Many attempts have been made to produce *holographic* images of the ionosphere, but it has not proven to be a very successful technique—probably because of the difficulty in uniformly illuminating a large enough horizontal slab of the ionosphere, not using a sufficient number of receivers, and the inability to achieve precise enough measurements of amplitude and phase of the reflected wave.

On the other hand, another technique (borrowed from medical technology), *computerized ionospheric tomography* (CIT), has produced quite significant results in imaging the regular (and some irregular) features of the ionosphere. Basically, this technique utilizes radio beacons on satellites in near-polar orbits and a latitudinal chain on the earth subsatellite path of carefully calibrated TEC receivers, to make many measurements of total electron content (TEC). The basic geometry is illustrated in Fig. 12.

Currently, VHF–UHF beacons on the TRANSIT, GLONASS, and GPS satellites are the most used as signal sources to measure TEC to use in CIT ionosphere reconstructions. One must also use some a priori information (ionospheric models) and ionosonde data in the algorithms in order to achieve realistic results. Some recent results are summarized in Refs. 33–38 and on the Internet at http://www.arlut.utexas.edu/~grk/Mace/mace.html and at http://sideshow.jpl.nasa.gov:80/gpsiono/.

Another ionospheric imaging technique is the IRIS system (Imaging Riometer-Ionospheric Studies) (46) which uses an antenna array of up to 64 elements to provide images of enhanced auroral absorption structure in the D-region.

Coherent Radars

As described in the subsection "Scattering of Radio Waves in the Ionosphere," HF–UHF coherent backscatter from ionospheric irregularities can provide very useful information on the morphology and physics of a wide range of irregularity scale sizes. At this time there are about 20 of these backscatter sounders deployed, operating on frequencies from ≈8 MHz to 200 MHz, distributed mainly in the high-latitude and equatorial regions. These radars are sited so that the main antenna lobe is directed to intercept irregularities at near-normal incidence at E- and F-region heights.

The HF coherent radars are mainly grouped into a large network, which covers approximately half of the northern polar cap ionosphere—the SuperDARN network (40), which is shown on the map in Fig. 13. Much information has been gained on the F-region plasma convection patterns in the polar cap, atmospheric gravity waves, and other ionospheric phenomena related to ionosphere magnetosphere interaction; see Refs. 40–42 or http://sd-www.jhuapl.edu/RADAR. The VHF–UHF coherent radars are documented in Refs. 2–5, and some useful Internet sources are to be found at http://dan.sp.

Table 2. Ionospheric Modification Facilities (1970 to 1978)

Facility	First Used	Latitude	Longitude	Geomag. Lat.	Transmit Power	Freq. Range (MHz)	Antenna Gain (dB)
Platteville, CO	1970	40.2°N	104.7°W	49°	1.6 MW	2.7–25	18
Arecibo, PR	1980	18°N	67°W	32°	800 kW	3–15	25
SURA, Russia	1980	56.1°N	46.1°E	71°	750 kW	4.5–9	26
Tromsoe, Norway	1980	69.6°N	19.2°E	67°	1.5 MW	2.5–8	28
HIPAS, Alaska	1977	64.9°N	146.8°W	65°	800 kW	2.8, 4.5	17
HAARP,[a] Alaska	1997	62.4°N	145.2°W	62°	3.6 MW[a]	2.8–10	30[a]

[a] HAARP is currently under construction. Values given are for the completed facility.

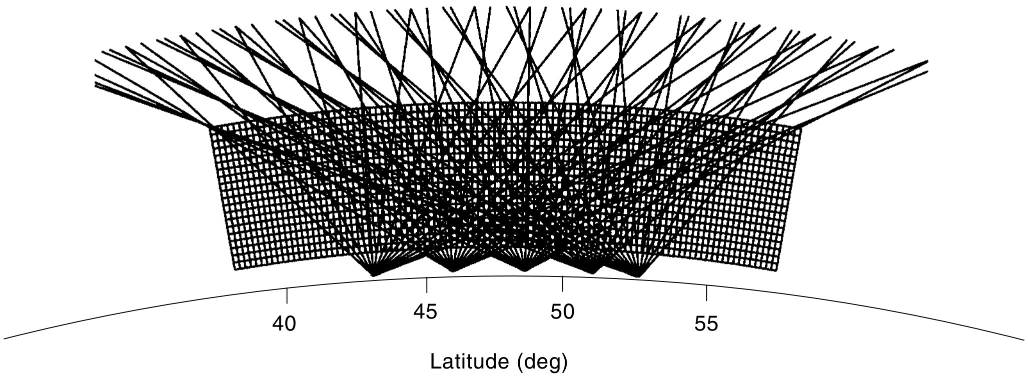

Figure 12. Basic satellite–earth geometry for computer ionospheric tomography, illustrating the multiple ray paths on which the total electron content is measured.

sp-agency.ca/www/cpus1e.htm, http://thor.ee.cornell.edu/~wes/CUPRI.

Incoherent Scatter Radars

One of the most powerful earth-based radio methods for studying the ionosphere is the *incoherent scatter radar* (ISR) technique, which has been in use since the early 1960s. ISRs can reveal the electron density, electron and ion temperature, plasma velocity, and other ionospheric parameters, even during very disturbed conditions (2–5). At the present time there are some seven ISRs in operation, located from the north polar cap to the magnetic equator and spread longitudinally from Scandinavia to Japan. The newest ISR is located at Svalbard, Norway (43), and another ISR is being planned for a polar observatory at Resolute, Canada in the near future

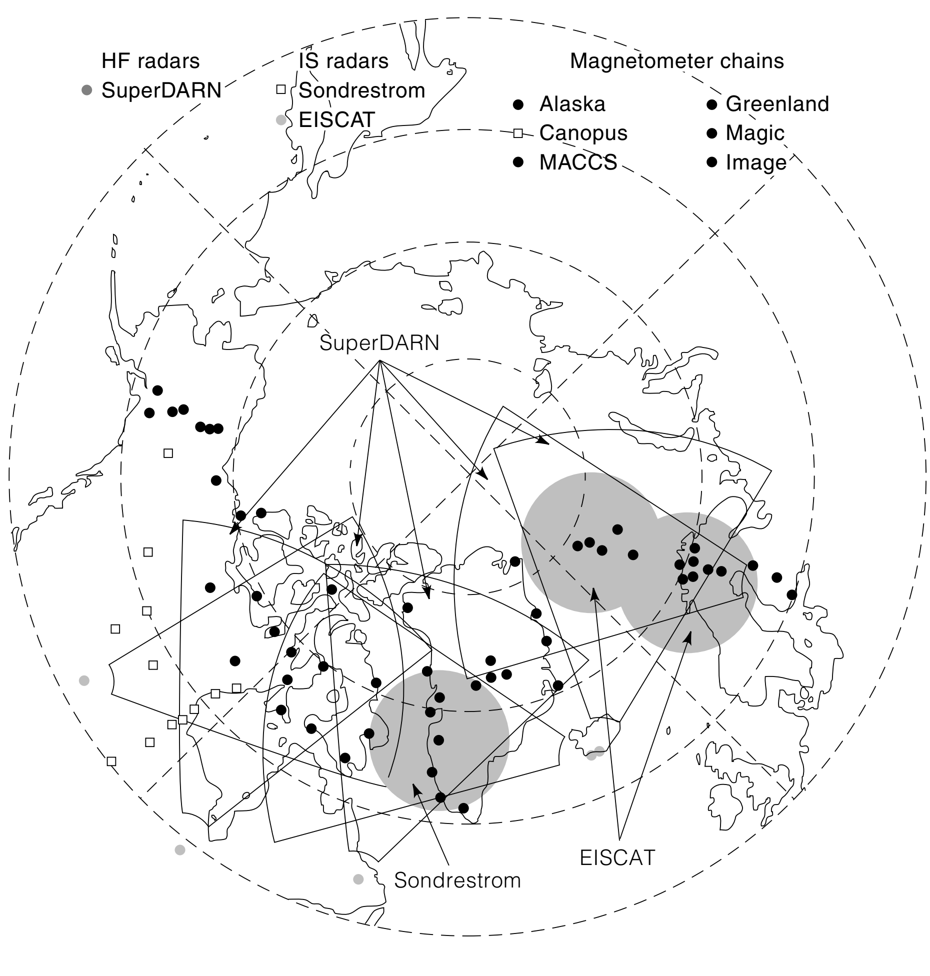

Figure 13. Northern hemisphere map showing area coverage of SuperDARN HF radars, incoherent scattering radars, and magnetometer chains. (Courtesy of R. A. Greenwald.)

(44). Data from ISRs are essential in studying the relation between the magnetosphere, ionosphere, and middle atmosphere at high and equatorial latitudes (47,48).

BIBLIOGRAPHY

1. H. Alfvén, *Cosmic Plasma,* Dordrecht, Holland: D. Reidel, 1981.
2. R. D. Hunsucker, *Radio Techniques for Probing the Terrestrial Ionosphere,* Heidelberg: Springer-Verlag, 1991.
3. R. D. Hunsucker, A review of ionospheric radio techniques: Present status and recent innovations, in W. R. Stone (ed.), *Review of Radio Science 1990–1992,* Oxford: Oxford Univ. Press, 1993, Chap. 22.
4. J. K. Hargreaves and R. D. Hunsucker, *The High-Latitude Ionosphere and its Effects on Radio Propagation,* Cambridge, UK: Cambridge Univ. Press, 1999, in press.
5. K. Davies, *Ionospheric Radio,* London: Peregrinus, 1990.
6. J. K. Hargreaves, *The Solar-Terrestrial Environment,* Cambridge, UK: Cambridge Univ. Press, 1992.
7. M. C. Kelley, *The Earth's Ionosphere—Plasma Physics and Electrodynamics,* San Diego, CA: Academic Press, 1989.
8. J. R. Wait, *Electromagnetic Waves in Stratified Media,* Oxford: Pergamon, 1970.
9. J. R. Wait, EM Scattering from a vertical column of ionization in the earth–ionosphere waveguide, *IEEE Trans. Antennas Propag.,* **39**: 1051–1054, 1991.
10. A. D. Watt, *VLF Radio Engineering,* Oxford: Pergamon, 1967.
11. R. D. Hunsucker and B. S. Delana, *High-latitude field-strength measurements of standard broadcast band skywave transmissions monitored at Fairbanks, Alaska,* Final Report on FCC Contract Number FCC-0375, Geophysical Institute/Univ. Alaska, 1988.
12. J. M. Goodman, *HF Communications—Science and Technology,* New York: Van Nostrand Reinhold, 1992.
13. E. E. Johnson et al., *Advanced High-Frequency Radio Communications,* Boston, MA: Artech House, 1997.
14. R. D. Hunsucker, Auroral and polar-cap ionospheric effects on radio propagation, *IEEE Trans. Antennas Propag.,* **40**: 818–828, 1992.
15. E. V. Appleton, Geophysical influence on the transmission of wireless waves, *Proc. Phys. Soc. London,* **37** (2): 16D–22D, 1925.
16. H. W. Nichols and J. C. Schelling, The propagation of electric waves over the earth, *Bell Syst. Tech. J.,* **4**: 215, 1925.
17. C. S. Gillmor and W. Altar, Edward Appleton and the magnetoionic theory, *Proc. Amer. Philos. Soc.,* **126** (5): 395–440, 1982.
18. W. H. Eccles, *Proc. R. Soc. London A, Math. Phys. Sci.,* **87**: 79, 1912.
19. J. M. Kelso, *Radio Ray Propagation in the Ionosphere,* New York: McGraw-Hill, 1964.
20. N. Smith, The relation of radio sky-wave transmission to ionospheric measurements, *Proc. IRE,* **27**: 332–347, 1939.
21. J. A. Ratcliffe, *The Magnetoionic Theory and Its Applications to the Ionosphere: A Monograph,* London: Cambridge Univ. Press, 1959.
22. K. Davies, *Ionospheric Radio Waves,* Waltham, MA: Blaisdell, 1969.
23. K. G. Budden, *The Propagation of Radio Waves. The Theory of Radio Waves of Low Power in the Ionosphere and Magnetosphere,* Cambridge, UK: Cambridge Univ. Press, 1985.
24. R. D. Hunsucker, Characteristic signatures of the midlatitude ionosphere observed with a narrow-beam HF backscatter sounder, *Radio Sci.,* **6**: 535–548, 1971.
25. R. A. Helliwell, *Whistlers and Related Ionospheric Phenomena,* Stanford, CA: Stanford Univ. Press, 1956.
26. D. Park and D. Carpenter, Very low frequency radio waves in the magnetosphere, in L. J. Lanzerotti and C. G. Parrs (eds.), *Upper Atmosphere Research in Antarctica,* Res. Ser. vol. 29, Monogr. 72, Washington: American Geophysical Union, 1978.
27. D. L. Carpenter, Remote sensing of the magnetospheric plasma by means of whistler mode signals, *Rev. Geophys.,* **26**: 535–549, 1988.
28. R. A. Helliwell, *VLF Whistler Mode Experiments,* Cambridge, MA: Cambridge Univ. Press, in press.
29. J. W. Wright, Jr. (ed.), *National Space Weather Program—Strategic Plan,* FCM-P30-1995, 1995, OFCMSSR; 8455 Colesville Rd. Suite 1500; Silver Spring, MD 20910.
30. *The National Space Weather Program—The Implementation Plan,* FCM-P31-1997, January 1997.
31. W. F. Utlaut (ed.), Special issue: Ionospheric modification by high power transmitters, *Radio Sci.,* **9**: 881–1089, 1974.
32. G. L. Rogers, A new method of analyzing ionospheric movement records, *Nature,* **177**: 613–614, 1956.
33. B. D. Wilson, Subdaily northern hemisphere ionospheric maps using an extensive network of GPS receivers, *Radio Sci.,* **30** (3): 639–648, 1995.
34. H. Na, J. Shen, and H. Lee, A Fourier domain technique for ionospheric tomography, *Radio Sci.,* **30** (3): 747–754, 1995.
35. M. Hernandez-Pojares, J. M. Juan, and J. Sanz, Neural network modeling of the ionospheric electron content at global scale using GPS data, *Radio Sci.,* **32** (3): 1081–1089, 1997.
36. L. Kersley et al., Imaging of electron density troughs by tomographic techniques, *Radio Sci.,* **32** (4): 1607–1621, 1997.
37. R. Leitinger, H.-P. Landreiter, and G. Kirchengast, Ionospheric tomography with data from satellite reception of Global Navigation Satellite system signals and ground reception of Navy Navigation satellite system signals, *Radio Sci.,* **32** (4): 1657–1667, 1997.
38. C. Coker, R. Hunsucker, and G. Lott, Detection of auroral activity using GPS satellites, *Geophys. Res. Lett.,* **22** (23): 3259–3262, 1995.
39. R. A. Greenwald et al., DARN/Superdarn: A global view of the dynamics of high-latitude convection, *Space Sci. Rev.,* **71**: 761–796, 1995.
40. R. A. Greenwald et al., Mesoscale dayside convection vortices and their relation to substorm phase, *J. Geophys. Res.,* **101** (A10): 21,697–21,713, 1996.
41. W. A. Bristow and R. A. Greenwald, On the spectrum of thermospheric gravity waves observed by the SuperDARN network, *J. Geophys. Res.,* **102** (A6): 11,585–11,595, 1997.
42. A. V. Kustov et al., Dayside ionospheric plasma convection, electric fields and field-aligned currents derived from the SuperDARN radar observations and predicted by the IZEMEM model, *J. Geophys. Res.,* **102** (A11): 24,057–24,067, 1997.
43. G. Wannberg et al., The EISCAT Svalbard radar: A case study in modern incoherent scatter radar system design, *Radio Sci.,* **32** (6): 2283–2307, 1997.
44. M.-C. Kelley (ed.), *A polar cap observatory: The next step in upper atmosphere science,* available from Ms. Sally Bird, The Theory Center, Room 304, Cornell Univ., Ithaca, NY 14853.
45. W. A. S. Murray and J. K. Hagreaves, Lunar radio echoes and the Faraday effect in the ionosphere, *Nature,* **173**: 944, 1954.
46. J. K. Hargreaves, D. L. Detrick, and T. J. Rosenberg, Space–time structure of auroral radio absorption events observed with Imaging-Riometer of South Pole, *Radio Sci.,* **26**: 925–930, 1991.
47. J. V. Evans , Ionospheric movement measured by ISR: A review. *J. Atmos. Terrestr. Phys.,* **34**: 175, 1972.

48. C. LaHoz (ed.), Special issue: Selected papers from the 6th Int. EISCAT Workshop, *J. Atmos. Terrestr. Phys.,* **58**: 1–507, 1996.

ROBERT D. HUNSUCKER
RP Consultants